

VS3R: Robust Full-frame Video Stabilization via Deep 3D Reconstruction

Muhua Zhu^{1*}, Xinhao Jin^{1*}, Yu Zhang¹, Yifei Xue¹, Tie Ji¹, and Yizhen Lao^{1**}

Hunan University, Changsha, Hunan 410082, China
{casmyzhu, jinxinhao, yuzhang, iflyhsueh, yizhenlao}@hnu.edu.cn,
jietie_hnu@163.com

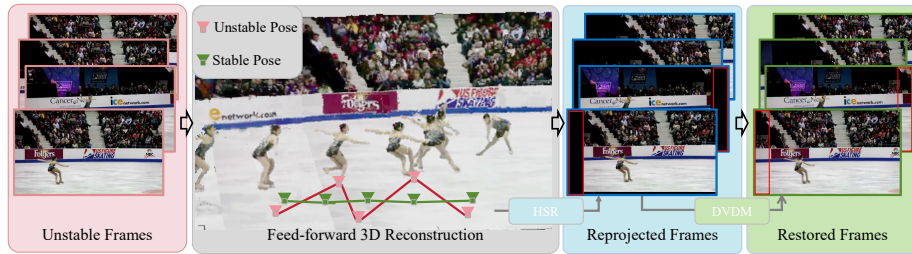


Fig. 1: We study the task of video stabilization from a novel 3D perspective. Given an uncalibrated video, we first reconstruct the local 3D scene using a feed-forward model. We then employ a hybrid rendering strategy, fusing semantic and geometric cues to synthesize stabilized frames. Finally, a dual-stream video diffusion model performs full-frame completion and refinement, producing high-fidelity, temporally coherent video.

Abstract. Video stabilization aims to mitigate camera shake but faces a fundamental trade-off between geometric robustness and full-frame consistency. While 2D methods suffer from aggressive cropping, 3D techniques are often undermined by fragile optimization pipelines that fail under extreme motions. To bridge this gap, we propose **VS3R**, a framework that synergizes feed-forward 3D reconstruction with generative video diffusion. Our pipeline jointly estimates camera parameters, depth, and masks to ensure all-scenario reliability, and introduces a **Hybrid Stabilized Rendering (HSR)** module that fuses semantic and geometric cues for dynamic consistency. Finally, a **Dual-Stream Video Diffusion Model (DVDM)** restores disoccluded regions and rectifies artifacts by synergizing structural guidance with semantic anchors. Collectively, VS3R achieves high-fidelity, full-frame stabilization across diverse camera models and significantly outperforms state-of-the-art methods in robustness and visual quality.

* Two authors contributed equally to this work.

** Corresponding author

Keywords: Video Stabilization · 3D Reconstruction · Diffusion Model

1 Introduction

Video stabilization aims to eliminate unintended camera shake induced by hand-held shooting or vehicle-mounted platforms [8]. A typical video stabilization pipeline comprises three core stages, namely, motion estimation of the unstable video, motion smoothing, and stabilized frame synthesis. Based on the underlying motion models employed for estimation, existing methods can be broadly categorized into 2D and 3D approaches.

Traditional **2D-based methods** typically employ planar transformations, such as affine [7], homography [18, 21, 26], or mesh-based warping [19, 21, 34], for frame alignment. While recent learning-based approaches attempt to implicitly estimate motion-compensated warping fields [4, 23, 39, 40, 44], they often struggle to generalize across diverse and complex scenarios due to data limitations. More critically, purely 2D stabilization methods lack physical constraints derived from the underlying 3D scene geometry. Consequently, these methods frequently fail in environments characterized by parallax, leading to severe structural distortions and temporal inconsistency as shown in Fig. 2(b). To hide these artifacts, 2D methods inevitably resort to aggressive cropping, resulting in a significant loss of field-of-view (shear in Fig. 2(a)) [7, 18].

To preserve structural integrity, Some **2.5D-based methods** incorporate depth cues [14] or subspace constraints [17] to enforce geometric consistency. Despite their ability to preserve scene structure, these 3D-aware methods frequently fail to synthesize full-frame content, often leaving behind projection artifacts or incomplete boundaries. Recently, **3D-based approaches** have emerged, leveraging paradigms such as NeRF [28] or 3D Gaussian Splatting [37] within reconstruct-and-render pipelines. However, these 3D methods heavily rely on standard Structure-from-Motion (SfM) for camera pose and depth estimation [28, 37]. SfM-based frameworks are inherently fragile in ill-posed scenarios, such as pure rotation or motion blur, where tracking often fails or suffers from severe scale drift due to geometric degeneracy, as depicted in Fig. 2(d) [37]. Furthermore, existing 3D techniques frequently struggle to synthesize full-frame content, often leaving behind projection artifacts or incomplete boundaries due to their limited handling of dynamic objects.

In summary, current stabilization paradigms face a fundamental trade-off between geometric robustness and full-frame consistency. While 2D-based temporal aggregation [4, 24, 28, 46] attempts to fill disoccluded regions to mitigate cropping-induced information loss, it frequently fails to maintain structural integrity, particularly under severe cropping (Fig. 2(c)). Conversely, although 3D-aware strategies incorporate depth priors [14, 20] or auxiliary sensors [15, 31] to enforce geometric fidelity, they often struggle with full-frame synthesis and projection artifacts. Most critically, emerging NeRF [28] and 3DGS [37] paradigms typically rely on decoupled pipelines, combining SfM with monocular depth, which triggers a cascading amplification of errors. This modularity renders them

fragile under geometric degeneracies (e.g., pure rotation) or aggressive motion scenarios, where traditional SfM frameworks suffer from tracking failures and learning-based estimators often drift.

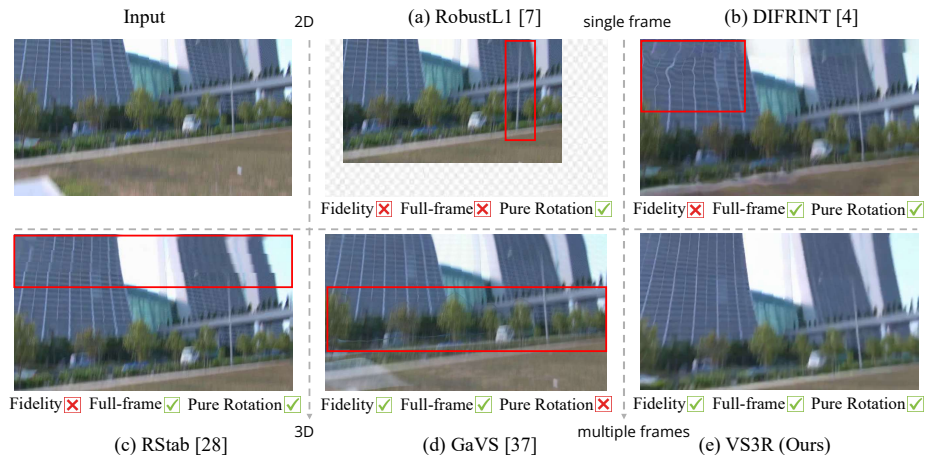


Fig. 2: Comparison of video stabilization paradigms in rapid pure-rotation scene, characterized by extreme motions, blur, and severe cropping. (a) 2D methods: Significant information loss due to aggressive cropping. (b) Learning-based: Geometric distortions and temporal flickering. (c) Completion-based: Failure in maintaining structural integrity. (d) SfM-based: Pose estimation failure under geometric degeneracy. (e) Ours: Full-frame, high-fidelity stabilization with robust geometric and temporal consistency.

Thus, there remains a critical need for a unified stabilization paradigm that concurrently delivers all-scenario robustness, high-fidelity full-frame synthesis, and temporal consistency across diverse scenes and complex camera motions.

To address the aforementioned challenges, we propose **VS3R** (Fig. 3), a novel and robust framework for video stabilization that leverages deep 3D reconstruction in conjunction with video diffusion models. **(1)** We first apply the feed-forward scene reconstruction model [10] to uncalibrated video frames, jointly recovering camera intrinsics, extrinsics, dynamic masks, and depth maps. To prevent global prediction drift and memory explosion typically associated with long-range sequences, we process the video sequence using a sliding window approach. Subsequently, we employ a Gaussian filter to smooth the camera trajectory. **(2)** Utilizing these optimized poses, we perform hybrid rendering of both static and dynamic points within the window to ensure geometric consistency. **(3)** To achieve full-frame restoration, we introduce a dual-stream video diffusion module that effectively completes missing details, compensates for cropped regions, and rectifies artifacts in the rendered sequence. Experimental results demonstrate that **VS3R** outperforms existing methods both qualitatively

and quantitatively, while simultaneously achieving full-frame synthesis, content and geometric preservation, and robustness across diverse scenes as shown in Fig. 2(e). [To facilitate reproducibility, the source code of VS3R is included in the supplementary material and is publicly available.](#) In summary, our contributions are summarized as:

- We propose a deep 3D reconstruction-based stabilization pipeline capable of generating full-frame videos with content, geometric, and temporal consistency under diverse and challenging camera motions.
- We introduce a Hybrid Stabilized Rendering (HSR) module that synergizes semantic and geometric cues to ensure consistency, complemented by a Dual-Stream Video Diffusion Model (DVDM) that restores disoccluded regions and rectifies artifacts via temporal aggregation, collectively achieving high-fidelity, full-frame stabilization without the need for aggressive cropping.
- Extensive experiments on public benchmarks demonstrate that VS3R significantly outperforms SOTA 2D and 3D methods. Our framework’s effectiveness is validated through quantitative metrics, qualitative comparisons, and a blind user study, showing superior robustness under extreme motions.

2 Related Work

•2D-based Video Stabilization. Earlier 2D methods typically model camera motion as a series of 2D transformations on the image plane, such as affine [7], homography [6, 18, 21, 26], feature tracks [11, 13, 22, 38], mesh flow [16, 19, 21] and dense flow [2, 4, 25, 45]. While efficient, these 2D-based approaches lack explicit 3D scene modeling, making them prone to geometric distortions in the presence of complex parallax. Furthermore, to avoid disoccluded regions, these methods inevitably rely on aggressive cropping, resulting in significant loss of field-of-view (FoV). Recent learning-based 2D methods [23, 40, 44] attempt to implicitly learn warping fields, yet they still struggle with the fundamental trade-off between stability and content preservation.

•2.5D and 3D-based Video Stabilization. To preserve structural integrity, some 2.5D-based approaches utilize additional hardware such as depth cameras [20] or IMUs [15, 31] to assist in recovering geometry. Some methods leverage depth cues [14] or subspace constraints [17] to enforce 3D-like consistency without full reconstruction. Recently, 3D-based methods have leveraged NeRF [28] or 3D Gaussian Splatting [37] to maintain geometric consistency through a reconstruct-and-render pipeline. However, their heavy reliance on standard SfM limits their robustness and generalization in ill-posed scenarios.

•Feed-forward 3D/4D Reconstruction and Conditional Generation. The recent progress in diffusion models [9, 30] has driven significant advancements in 3D/4D reconstruction and conditional video generation. Building on pioneering works such as ControlNet [42] and T2I-Adapter [27], which introduced various conditional signals for image generation, similar strategies have been extended to video synthesis to enable controls via depth [5], trajectories [36], and

RGB images [1]. Inspired by these reconstruction-based novel view synthesis methods [3,41], we leverage conditional video diffusion models [1,33] to address the long-standing challenges in video stabilization. Specifically, our approach utilizes 3D structural priors as conditioning signals to rectify cropping artifacts and temporal inconsistencies, ensuring high-fidelity full-frame restoration.

3 Methodology

3.1 pipeline

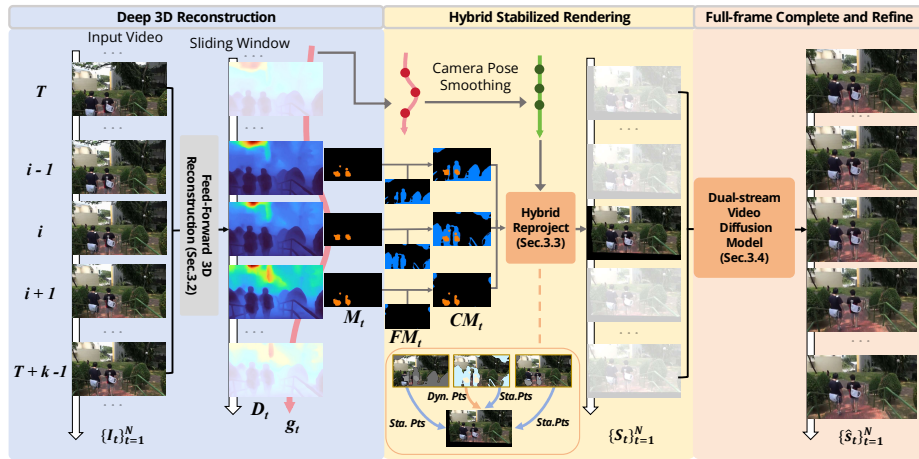


Fig. 3: Overview of the VS3R pipeline. VS3R follows a "reconstruct-smooth-refine" paradigm: (1) Deep 3D Reconstruction (Sec. 3.2): Estimates camera parameters g_t , semantic masks M_t , and depth D_t from uncalibrated video via a feed-forward model [10]. (2) Hybrid Stabilized Rendering (Sec. 3.3): Refines dynamic mask CM_t by merging M_t with geometric mask FM_t , then renders stabilized frames S_t along the smoothed trajectory. (3) Full-frame Refinement (Sec. 3.4): A dual-stream diffusion model restores disoccluded regions and rectifies artifacts to produce high-fidelity, temporally coherent frames \hat{S}_t .

Fig. 3 illustrates the overall architecture of our VS3R framework. To overcome the limitations of traditional SfM-based methods and 2D warping, VS3R adopts a robust "reconstruct-smooth-refine" paradigm consisting of the following three core steps: **(1) Deep 3D Scene Reconstruction.** Given an uncalibrated unstable video sequence, we first employ a feed-forward deep reconstruction model [10] to jointly recover camera intrinsics, extrinsics, dynamic masks, and depth maps, as detailed in Sec. 3.2. **(2) Hybrid Stabilized Rendering.** To produce a stabilized video, we apply a Gaussian filter to the estimated camera trajectory to obtain a smoothed path. Subsequently, we perform hybrid rendering of both static scene elements and dynamic objects within the window,

as elaborated in Sec. 3.3. **(3) Full-frame Completion and Refinement.** The preliminary rendered frames often suffer from cropping artifacts and disoccluded regions at the boundaries. To achieve full-frame stabilization, we introduce a Dual-stream video diffusion model, as depicted in Sec. 3.4.

3.2 Deep 3D Reconstruction

Unlike traditional 3D stabilization methods that rely on fragile Structure-from-Motion (SfM) optimization, we adopt a feed-forward deep 4D reconstruction paradigm VGGT4D [10] to ensure robustness in challenging scenarios. As shown in Fig. 3, to facilitate long-range processing while mitigating global drift, the input RGB sequence $\mathcal{I} = \{I_i\}_{i=1}^N$ is handled via a sliding window approach. Specifically, we leverage VGGT4D [10] to jointly estimate camera parameters, scene structure, and temporal correspondences. The reconstruction process for a given window is formulated as:

$$\mathcal{F}(\{I_i\}_{i=T}^{T+W-1}) = \{\mathbf{g}_i, D_i, P_i, M_i\}_{i=T}^{T+W-1}, \quad (1)$$

where W denotes the window size. For each frame i , \mathbf{g}_i represents the camera’s intrinsic K_i and extrinsic parameters T_i , D_i is the predicted per-pixel depth map, P_i signifies the corresponding 3D point map, and M_i represents the **semantic-driven dynamic mask**. However, while the feed-forward model leverages deep semantic priors to estimate object-level motion, these masks often exhibit inaccuracies or temporal inconsistencies, potentially leading to severe visual artifacts during the hybrid rendering process. The subsequent section will detail the Hybrid Stabilized Rendering (HSR) module, which utilizes these predictions to eliminate the aforementioned artifacts and ensure geometric consistency.

3.3 Hybrid Stabilized Rendering

Camera Path Smoothing. To derive stabilized camera trajectories from the raw parameters \mathbf{g}_i , following [14], we apply temporal Gaussian smoothing to both translation and rotation components:

$$\hat{\mathbf{g}}_k = \sum_{i=k-r}^{k+r} \omega(i, k) \mathbf{g}_i \quad (2)$$

$$\omega(i, k) = \exp\left(-\frac{(i-k)^2}{2\sigma^2}\right) \quad (3)$$

where r denotes the temporal radius and $\omega(i, k)$ represents the normalized Gaussian weights. For rotation, filtering is performed in unit quaternion space with sign-alignment to preserve motion continuity. By tuning the bandwidth parameter σ , our system synthesizes videos with varying degrees of stabilization.

Hybrid Dynamic Mask. To suppress potential artifacts from moving objects, we refine the dynamic mask by merging the semantic-aware dynamic mask M_t and geometric dynamic mask FM_t . To obtain FM_t , we first define the induced rigid flow \mathbf{f}_r^t at pixel \mathbf{p} . Intuitively, \mathbf{f}_r^t represents the expected pixel motion caused solely by the camera’s ego-motion, assuming the underlying 3D scene is completely stationary. This projected motion field under the static scene assumption is formulated as::

$$\mathbf{f}_r^t(\mathbf{p}) = K [R_{t+1}^{-1} ((R_t K^{-1} \mathbf{p} D_t + \mathbf{t}_t) - \mathbf{t}_{t+1})] - \mathbf{p} \quad (4)$$

where K denotes the camera intrinsic, and $\{R_t, \mathbf{t}_t\}$ represents the camera rotation and translation that transform a point from the camera coordinate system to the world coordinate system. D_t is the depth of frame t . The geometric flow mask FM_t is then determined by thresholding the ℓ_2 -norm of the residual between the observed optical flow \mathbf{f}_o^t , which is robustly estimated using the pre-trained RAFT Large model [32], and the induced rigid motion \mathbf{f}_r^t :

$$FM_t(\mathbf{p}) = \mathbb{I}(\|\mathbf{f}_o^t(\mathbf{p}) - \mathbf{f}_r^t(\mathbf{p})\|_2 > \tau) \quad (5)$$

where $\mathbb{I}(\cdot)$ is the indicator function and τ is a distance threshold. The final combined mask CM_t is obtained by the logical union of the semantic mask M_t and the geometric mask FM_t , expressed as $CM_t = M_t \vee FM_t$. This hybrid strategy ensures that pixels violating the static scene assumption—detected via semantic priors or cross-frame geometric inconsistencies—are consistently identified as dynamic regions for the subsequent rendering stage.

Hybrid Reprojection. To synthesize the stabilized frame S_t , we represent the scene as a composite 3D point cloud. Based on the mask CM_t , we distinguish between static and dynamic regions to aggregate a global-local point set \mathcal{P}_t :

$$\mathcal{P}_t = \mathcal{P}_t^s \cup \mathcal{P}_t^d \quad (6)$$

where the static component $\mathcal{P}_t^s = \{P_i(\mathbf{p}) \mid i \in \mathcal{N}(t), CM_i(\mathbf{p}) = 0\}$ aggregates spatial information across a temporal window $\mathcal{N}(t)$ of size n to fill disocclusion gaps and suppress artifacts through multi-view consistency. Conversely, the dynamic component $\mathcal{P}_t^d = \{P_t(\mathbf{p}) \mid CM_t(\mathbf{p}) = 1\}$ is restricted to the current frame t to preserve the temporal integrity of non-rigid motion. The final stabilized frame S_t is rendered by projecting the composite point cloud \mathcal{P}_t using the smoothed camera pose $\hat{\mathbf{g}}_t$:

$$S_t = \mathcal{R}(\mathcal{P}_t, \hat{\mathbf{g}}_t, K) \quad (7)$$

where $\mathcal{R}(\cdot)$ denotes the point-based rendering operation implemented via PyTorch3D [29], and K represents the camera intrinsic matrix.

This hybrid stabilized rendering mechanism ensures that the rendered output maintains both geometric stability and temporal coherence. Nevertheless, the transformation of camera poses inevitably introduces artifacts such as cropped boundaries, disocclusion holes, and sampling noise. These challenges are addressed in the subsequent section, which introduces a dual-stream video diffusion model to complete and optimize the geometry-preserved frames S_t .

3.4 Full-frame Completion and Refinement

While the hybrid reprojection module produces geometrically stable frames S_t , the sequence often exhibits cropping artifacts, occlusion holes, and rendering noise. To reconstruct high-fidelity full-frame videos, we propose a **Dual-stream Video Diffusion Model** that synergizes structural priors with semantic guidance to achieve joint restoration and refinement. The model incorporates two distinct input streams: (1) A Video Conditioning Stream that utilizes the rendered frames $\{S_t\}_{t=1}^N$ to provide spatial priors and motion trajectories. (2) A Global Semantic Stream that employs a fixed, universal text embedding to serve as a semantic anchor. This stream guides the model to maintain consistent visual quality and aesthetic style across diverse scenes. By fusing these streams, the model effectively borrows information from neighboring frames to fill disocclusion holes and rectify rendering noise, synthesizing a temporally coherent, full-frame video $\{\hat{S}_t\}_{t=1}^N$.

Data Curation. To facilitate model training, we curated a dataset based on the NUS [21], comprising pairs of degraded stable videos and their clean counterparts. Specifically, we simulate realistic degradations—including cropping boundaries, occlusion holes, and rendering noise—onto the reprojected frames to bridge the gap between synthetic and real-world artifacts. By pairing these synthetically degraded videos with the original high-quality sequences as ground truth, we establish a robust training corpus for fine-tuning our video diffusion model. **Furthermore**, evaluations on the DeepStab [34] datasets confirm our model’s robust generalization without data leakage (see Appendix Sec. A).

Fine-tuning. Our restoration model is built upon the Wan2.2-I2V-14B framework [33], featuring a Dual-DiT Mixture-of-Experts (MoE) architecture as shown in Fig. 4. We employ the Wan-VAE encoder \mathcal{E} to compress the degraded video $V^{degrade}$ and target video V^{target} into latents $\mathbf{z}_{degrade}$ and \mathbf{z}_{target} , respectively. Following Flow Matching, the noisy latent \mathbf{z}_t is constructed via linear interpolation:

$$\mathbf{z}_t = (1 - t)\epsilon + t\mathbf{z}_{target} \quad (8)$$

where $t \in [0, 1]$ is the normalized timestep and $\epsilon \sim \mathcal{N}(0, \mathbf{I})$. To adapt the image-to-video setting for enhancement, we concatenate the full-sequence $\mathbf{z}_{degrade}$ with \mathbf{z}_t along the channel axis to guide the restoration of artifacts and holes. During fine-tuning, the VAE is frozen, and LoRA-based adaptation is applied exclusively to the Transformer experts within the MoE structure. This preserves pre-trained generative priors while learning the mapping to clean videos. The training objective is defined by the Flow Matching loss:

$$\mathcal{L}_{tune} = \mathbb{E}_{\mathbf{z}_{target}, t, \epsilon, \mathbf{z}_{degrade}} \left[\|\mathbf{v}_\theta(\mathbf{z}_t, t, \mathbf{z}_{degrade}, c_{tex}) - (\epsilon - \mathbf{z}_{target})\|_2^2 \right] \quad (9)$$

where \mathbf{v}_θ is the predicted velocity and c_{tex} is a global task-oriented prompt ensuring high-fidelity, artifact-free synthesis.

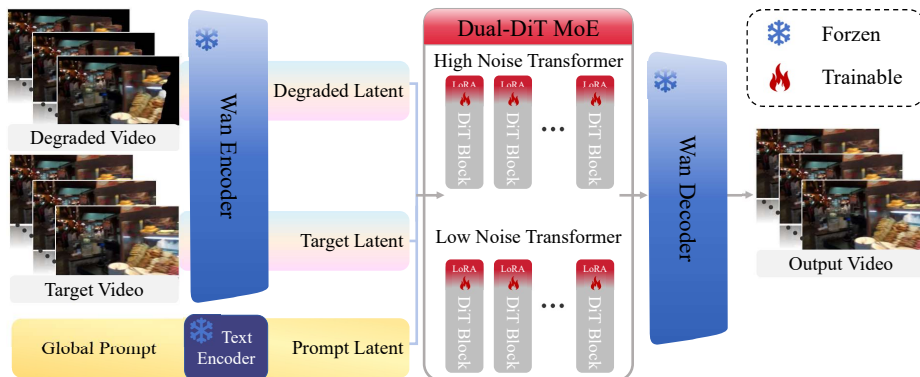


Fig. 4: Architecture of the dual-stream video diffusion model. To facilitate efficient fine-tuning, we freeze all network parameters except for the LoRA weights. Specifically, LoRA layers with a rank of 32 are integrated into every transformer block within the two DiT models.

Implementation Details. We fine-tune the Dual-DiT backbone of Wan2.2 via Low-Rank Adaptation (LoRA). Specifically, LoRA modules are integrated into the linear projections of both the attention mechanisms and the feed-forward networks. The model is trained on our curated dataset of noisy-clean video pairs using the AdamW optimizer with a learning rate of $\eta = 1 \times 10^{-4}$ and a weight decay of 10^{-2} . Both the LoRA rank and alpha are set to 32. To facilitate detail restoration under high-noise regimes, we implement a shifted timestep sampling strategy with a shift factor of 5.0. The Dual-DiT MoE model is jointly trained on 4 NVIDIA H20 GPUs for 10 epochs using bf16 mixed precision, totaling approximately 560 GPU hours.

4 Experiments

4.1 Experimental Setting

Datasets. We evaluate our method on public dataset NUS [21]. The NUS dataset comprises 144 videos, categorized into six different scenes: Regular, Running, Crowd, Parallax, QuickRotation, and Running. **Furthermore**, cross-dataset evaluations on the unseen DeepStab [34] dataset confirm our model’s robust generalization without data leakage (as shown in Appendix Sec. A).

Baseline. We choose various video stabilization algorithms as the baselines, including RobustL1 [7], Bundled [21], Yu et al. [40], DIFRINT [4], DUT [35], Rstab [28] and GaVS [37]. For comparisons, we use the videos generated by official implementations with default parameters or pre-trained models.

Metrics. We assess Cropping and Stability scores following the method in [4], alongside the Epipolar Sampson Error (ESE), Warping Error (WE) [12], and

LPIPS [43]: (1) **Cropping Ratio**: Measures the remaining image area after removing non-content pixels. (2) **Stability Score**: Assesses smoothness via the ratio of low-frequency to total motion energy. (3) **Epipolar Sampson Error (ESE)**: Quantifies geometric consistency by measuring point-to-epipolar-line distances across consecutive frames. (4) **Warping Error (WE)**: Evaluates temporal coherence using mean squared error between frames warped via dense optical flow. (5) **LPIPS**: Measures perceptual similarity through deep feature comparison after image registration to ensure high-fidelity reconstruction.

Notably, we replace traditional distortion metrics with the ESE-WE-LPIPS triplet. Since global homography-based estimation is ill-suited for videos with significant scene depth and parallax, it fails to provide a reliable measure of geometric deformation in 3D-complex environments. Instead, this combination more reliably characterizes geometric consistency, temporal stability, and visual fidelity in 3D-complex scenes.

4.2 Qualitative Results

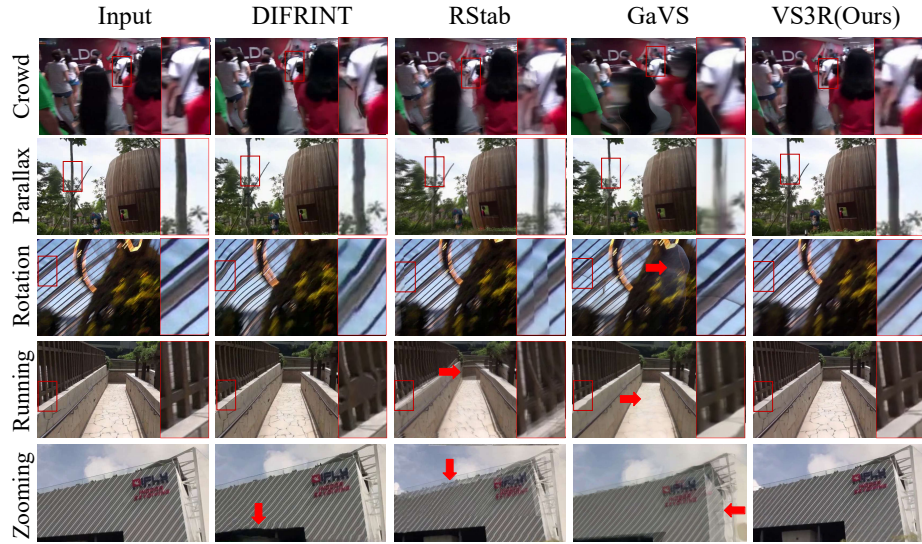


Fig. 5: Qualitative comparison of stabilized video on NUS [21] dataset. Our VS3R generates stabilized videos with significantly higher content, geometric, and temporal consistency compared to existing state-of-the-art methods, including DIFRINT [4], Rstab [28], and GaVS [37], across various challenging scenarios.

Fig. 5 illustrates representative artifacts, distortions, and algorithmic failures observed across different methods. Due to their 2D full-frame completion paradigms, **DIFRINT** and **Rstab** suffer from significant blurring and distortions at frame boundaries under rapid camera motion, where aggressive cropping

is required. While **Gavs** attempts to address these issues via 2D outpainting and 3D rendering, it is often hindered by the limitations of traditional Structure-from-Motion (SfM) preprocessing, leading to performance degradation in extreme cases such as *quick rotation* and *zooming*. In contrast, our **VS3R** method consistently generates stable frames with significantly more complete structures and fewer severe distortions in these complex and challenging scenarios.

4.3 Quantitative Evaluation

Table 1: Quantitative comparison of video stabilization on the NUS [21]. We evaluate our method against baselines using five metrics: Cropping, Stability, LPIPS, Epipolar Sampson Error(ESE), Warping Error(WE). The **best** and **second best** results are highlighted in green and blue, respectively.

| Type | Method | Average of All Categories | | | | |
|------------|----------------|---------------------------|----------------------|--------------------|--------------------------------|----------------------------------|
| | | Cropping \uparrow | Stability \uparrow | LPIPS \downarrow | ESE ($pixel^2$) \downarrow | WE($\times 1e-3$) \downarrow |
| Normal | Bundled [21] | 0.978 | 0.864 | 0.129 | 120.1 | 1.357 |
| | RobustL1 [7] | 0.819 | 0.846 | 0.109 | 83.6 | 1.044 |
| | Yu et al. [40] | 0.881 | 0.860 | 0.149 | 119.5 | 1.266 |
| | DUT [35] | 0.875 | 0.897 | 0.102 | 93.4 | 1.084 |
| Full-frame | DIFRINT [4] | 0.964 | 0.849 | 0.131 | 88.0 | 1.262 |
| | Rstab [28] | 0.989 | 0.864 | 0.136 | 87.5 | 1.145 |
| | GaVS [37] | 0.999 | 0.841 | 0.181 | 95.6 | 1.149 |
| | VS3R (Ours) | 1.000 | 0.901 | 0.170 | 61.7 | 0.991 |

| Type | Method | Crowd | | | | | Parallax | | | | | Rotation | | | | |
|------------|----------------|--------------|--------------|----------------|------------------|-----------------|--------------|--------------|----------------|------------------|-----------------|--------------|--------------|----------------|------------------|-----------------|
| | | C \uparrow | S \uparrow | L \downarrow | ESE \downarrow | WE \downarrow | C \uparrow | S \uparrow | L \downarrow | ESE \downarrow | WE \downarrow | C \uparrow | S \uparrow | L \downarrow | ESE \downarrow | WE \downarrow |
| Normal | Bundled [21] | 0.998 | 0.834 | 0.073 | 128.6 | 1.250 | 0.989 | 0.841 | 0.111 | 147.6 | 1.486 | 0.904 | 0.900 | 0.272 | 121.0 | 1.323 |
| | RobustL1 [7] | 0.817 | 0.867 | 0.059 | 94.3 | 0.968 | 0.817 | 0.857 | 0.058 | 103.7 | 1.248 | 0.821 | 0.891 | 0.070 | 92.8 | 1.184 |
| | Yu et al. [40] | 0.903 | 0.872 | 0.150 | 101.7 | 1.123 | 0.884 | 0.812 | 0.160 | 125.3 | 1.454 | 0.860 | 0.896 | 0.146 | 164.2 | 1.493 |
| | DUT [35] | 0.874 | 0.906 | 0.085 | 92.4 | 1.041 | 0.874 | 0.878 | 0.092 | 115.1 | 1.319 | 0.876 | 0.896 | 0.097 | 106.3 | 1.337 |
| Full-frame | DIFRINT [4] | 0.961 | 0.809 | 0.134 | 92.1 | 1.258 | 0.964 | 0.829 | 0.127 | 107.5 | 1.470 | 0.971 | 0.907 | 0.132 | 106.8 | 1.345 |
| | Rstab [28] | 0.978 | 0.823 | 0.101 | 79.2 | 1.152 | 0.944 | 0.840 | 0.142 | 196.7 | 1.290 | 0.999 | 0.908 | 0.147 | 79.8 | 1.335 |
| | GaVS [37] | 1.000 | 0.812 | 0.132 | 65.9 | 1.115 | 1.000 | 0.845 | 0.146 | 90.2 | 1.338 | 0.999 | 0.913 | 0.134 | 73.8 | 1.245 |
| | VS3R (Ours) | 0.999 | 0.878 | 0.167 | 51.1 | 0.979 | 1.000 | 0.909 | 0.151 | 96.0 | 1.199 | 0.999 | 0.917 | 0.159 | 77.2 | 1.172 |

| Type | Method | Regular | | | | | Running | | | | | Zooming | | | | |
|------------|----------------|--------------|--------------|----------------|------------------|-----------------|--------------|--------------|----------------|------------------|-----------------|--------------|--------------|----------------|------------------|-----------------|
| | | C \uparrow | S \uparrow | L \downarrow | ESE \downarrow | WE \downarrow | C \uparrow | S \uparrow | L \downarrow | ESE \downarrow | WE \downarrow | C \uparrow | S \uparrow | L \downarrow | ESE \downarrow | WE \downarrow |
| Normal | Bundled [21] | 1.000 | 0.839 | 0.121 | 76.2 | 1.058 | 0.997 | 0.866 | 0.089 | 111.2 | 1.761 | 0.995 | 0.888 | 0.092 | 137.7 | 1.327 |
| | RobustL1 [7] | 0.820 | 0.895 | 0.089 | 44.3 | 0.653 | 0.821 | 0.882 | 0.069 | 65.7 | 1.152 | 0.819 | 0.907 | 0.069 | 97.9 | 1.066 |
| | Yu et al. [40] | 0.912 | 0.915 | 0.141 | 57.0 | 0.858 | 0.880 | 0.840 | 0.167 | 110.4 | 1.560 | 0.860 | 0.836 | 0.137 | 142.0 | 1.135 |
| | DUT [35] | 0.874 | 0.882 | 0.131 | 53.7 | 0.686 | 0.874 | 0.901 | 0.101 | 82.1 | 1.077 | 0.878 | 0.911 | 0.104 | 107.9 | 1.041 |
| Full-frame | DIFRINT [4] | 0.961 | 0.794 | 0.142 | 49.0 | 0.883 | 0.961 | 0.836 | 0.126 | 63.0 | 1.485 | 0.966 | 0.890 | 0.123 | 103.8 | 1.183 |
| | Rstab [28] | 1.000 | 0.845 | 0.152 | 46.3 | 0.780 | 0.999 | 0.861 | 0.135 | 60.3 | 1.189 | 1.000 | 0.886 | 0.139 | 87.5 | 1.117 |
| | GaVS [37] | 1.000 | 0.821 | 0.179 | 42.7 | 0.778 | 0.999 | 0.829 | 0.161 | 53.8 | 1.363 | 0.996 | 0.814 | 0.306 | 218.1 | 1.097 |
| | VS3R (Ours) | 1.000 | 0.913 | 0.192 | 25.4 | 0.556 | 1.000 | 0.894 | 0.178 | 37.6 | 0.933 | 1.000 | 0.895 | 0.171 | 80.5 | 1.082 |

Tab. 1 presents the average results for six categories on the NUS dataset. As shown in Tab. 1, **VS3R** achieves significant performance improvements over existing video stabilization methods.

Regarding stability, our method’s tolerance to cropping allows for larger smoothing bandwidths, which leads to superior stability. In terms of consistency, our approach outperforms other methods in both geometric and temporal coherence. While our LPIPS scores may trail 2D methods, this is inherent to 3D-based stabilization. First, perspective warps from pose optimization prevent

perfect pixel alignment, causing LPIPS to misinterpret geometric shifts as distortion. Second, the 3D re-rendering process inevitably introduces minor pixel residuals. However, our user study confirms these shifts do not affect visual quality, representing a necessary trade-off for superior 3D consistency.

4.4 User Study

We conducted a user study to compare our method with several state-of-the-art full-frame approaches, namely DIFRINT [4], Rstab [28], and Gavs [37]. Specifically, we prepared a test set consisting of 18 video sequences (3 videos per category). We recruited 16 participants for a blind user study. For each test case, participants were presented with the original unstable video as a reference and asked to select the most visually pleasing result among the four randomized competing methods. The statistical results of this user study are illustrated in Fig. 6, demonstrating that our method is consistently preferred by users.

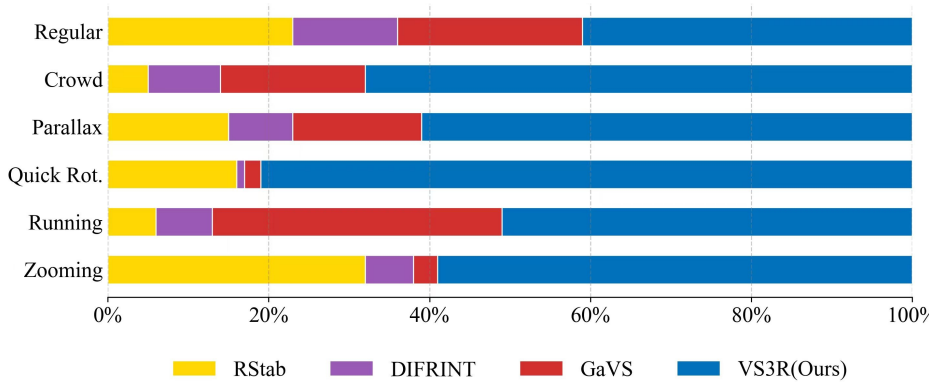


Fig. 6: User preference test results on 6 video categories.

4.5 Ablation Study

We evaluate the contributions of the Hybrid Stabilized Rendering (HSR) and Dual-stream Video Diffusion Model (DVDM) modules. Experiments are conducted on the dynamic Crowd scene from the NUS dataset [21], selected for its complex motions and dynamic environments.

Effectiveness of HSR. We validate HSR by comparing it against a baseline (Fig. 7(a)) that renders solely on raw dynamic masks M_t from VGGT4D [10]. As illustrated in Fig. 7(a) and Tab. 2, inaccuracies in network-predicted masks lead to significant rendering artifacts. By integrating semantic-driven mask M_t with geometric mask FM_t , HSR effectively mitigates these errors, maintaining



Fig. 7: Qualitative ablation of HSR and DVDM. (b) w/o HSR: Artifacts and structural instability arise from relying solely on predicted masks. (c) w/o DVDM: Results exhibit disocclusion holes and texture loss without diffusion-based completion. (d) Full (Ours): HSR ensures geometric stability in dynamic regions, while DVDM restores disoccluded areas with temporal coherence and high fidelity.

structural integrity and suppressing artifacts in dynamic regions.

Effectiveness of DVDM. The role of DVDM is analyzed by excluding the diffusion-based refinement process. Without DVDM, the rendered frames suffer from disocclusion holes and missing textures as shown in Fig. 7(b) and Tab. 2, as geometric projection alone cannot synthesize unseen content. In contrast, DVDM leverages its dual-stream architecture to fill these gaps while enforcing temporal consistency. Results demonstrate that DVDM significantly enhances perceptual quality, producing photo-realistic stabilized videos.

Table 2: Quantitative ablation study of HSR and DVDM modules. We conduct comparative experiments of the effect of each module. The **best** and **second best** results are highlighted in green and blue, respectively.

| Method | Cropping \uparrow | Stability \uparrow | LPIPS \downarrow | ESE ($pixel^2$) \downarrow | WE ($\times 1e-3$) \downarrow |
|------------|---------------------|----------------------|--------------------|--------------------------------|-----------------------------------|
| Baseline | 0.994 | 0.874 | 0.231 | 123.3 | 1.383 |
| w/o HSR | 1.000 | 0.892 | 0.197 | 89.6 | 1.135 |
| w/o DVDM | 0.987 | 0.887 | 0.214 | 115.3 | 1.128 |
| Full(Ours) | 1.000 | 0.901 | 0.170 | 61.7 | 0.991 |

5 Discussion

- **Why deep 3DR?** Explicit 3D reconstruction is crucial for understanding scene geometry. Compared to traditional Structure-from-Motion (SfM), feed-forward neural networks offer more robust camera pose and depth estimation. They effectively prevent tracking failures and scale ambiguity, especially under extreme camera motions.
- **Why video diffusion model?** Extreme camera motion causes severe cropping, where neighboring frames often lack sufficient information to fill large disocclusions. Fine-tuned Video Diffusion Models solve this by enforcing structural coherence. By combining temporal context from adjacent frames with their generative priors, they synthesize missing content with high fidelity.

- **Application?** **VS3R** generates artifact-free, full-frame stabilized videos with cinematic quality. By decoupling motion from geometry, it preserves visual consistency and flexibly renders outputs for various camera models as shown in Fig. 8.

- **Limitation?** Despite its effectiveness, **VS3R** has limitations. *(1)*Reliance on Deep 3DR: Our framework relies on robust poses and accurate depth. However, intense depth fluctuations can introduce temporal jitter, a characteristic challenge for 3D stabilization in highly dynamic scenes. *(2)*Fidelity Constraints: Pre-trained diffusion models may occasionally degrade fine textures. Though perceptual impact is minimal, future foundation models will improve output precision. *(3)*Computational Overhead: Achieving state-of-the-art full-frame consistency demands substantial resources. While inference time is on par with 3D stabilizers, our framework requires higher VRAM (Appendix Sec. B). This memory trade-off is justified by our strictly superior stabilization and visual quality. Future optimizations will explore lightweight diffusion models and efficient sampling to reduce this overhead.

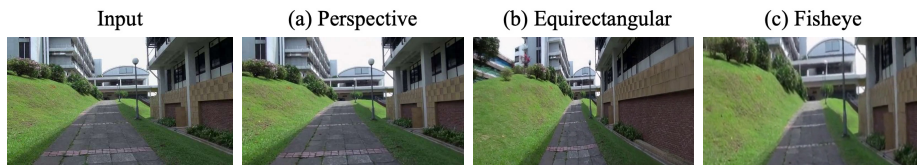


Fig. 8: Flexibility across diverse camera models. VS3R supports rendering stabilized videos through various camera models, including perspective, fisheye, and equirectangular projections.

6 Conclusion

In this paper, we introduced **VS3R**, a robust video stabilization framework that effectively addresses the fundamental trade-off between geometric robustness and full-frame consistency. By synergizing deep 3D reconstruction with generative video diffusion, our approach transcends the limitations of traditional 2D warping and fragile SfM-based optimization pipelines. Through a feed-forward reconstruction network and a **HSR** module, we ensure geometric fidelity and dynamic consistency even in challenging, unconstrained environments. Furthermore, our **DVDM** enables high-fidelity full-frame restoration by rectifying projection artifacts and disocclusion holes without cropping. Extensive qualitative and quantitative evaluations, supported by a user study, demonstrate that **VS3R** significantly outperforms state-of-the-art methods.

References

1. Blattmann, A., Dockhorn, T., Kulal, S., Mendeleevitch, D., Kilian, M., Lorenz, D., Levi, Y., English, Z., Voleti, V., Letts, A., et al.: Stable video diffusion: Scaling latent video diffusion models to large datasets. arXiv preprint arXiv:2311.15127 (2023)
2. Chen, Y.T., Tseng, K.W., Lee, Y.C., Chen, C.Y., Hung, Y.P.: Pixstabnet: Fast multi-scale deep online video stabilization with pixel-based warping. In: 2021 IEEE International Conference on Image Processing (ICIP). pp. 1929–1933. IEEE (2021)
3. Chen, Y., Guo, S., Yang, T., Ding, L., Yu, X., Gu, J., Xue, T.: 4dslomo: 4d reconstruction for high speed scene with asynchronous capture. In: Proceedings of the SIGGRAPH Asia 2025 Conference Papers. pp. 1–11 (2025)
4. Choi, J., Kweon, I.S.: Deep iterative frame interpolation for full-frame video stabilization. *ACM Trans. Graph.* **39**(1) (Jan 2020). <https://doi.org/10.1145/3363550>, <https://doi.org/10.1145/3363550>
5. Esser, P., Chiu, J., Atighehchian, P., Granskog, J., Germanidis, A.: Structure and content-guided video synthesis with diffusion models. In: Proceedings of the IEEE/CVF international conference on computer vision. pp. 7346–7356 (2023)
6. Goldstein, A., Fattal, R.: Video stabilization using epipolar geometry. *ACM Transactions on Graphics (TOG)* **31**(5), 1–10 (2012)
7. Grundmann, M., Kwatra, V., Essa, I.: Auto-directed video stabilization with robust l1 optimal camera paths. In: CVPR 2011. pp. 225–232. IEEE (2011)
8. Guilluy, W., Oudre, L., Beghdadi, A.: Video stabilization: Overview, challenges and perspectives. *Signal Processing: Image Communication* **90**, 116015 (2021)
9. Ho, J., Jain, A., Abbeel, P.: Denoising diffusion probabilistic models. *Advances in neural information processing systems* **33**, 6840–6851 (2020)
10. Hu, Y., Cheng, C., Yu, S., Guo, X., Wang, H.: Vggt4d: Mining motion cues in visual geometry transformers for 4d scene reconstruction. arXiv preprint arXiv:2511.19971 (2025)
11. Koh, Y.J., Lee, C., Kim, C.S.: Video stabilization based on feature trajectory augmentation and selection and robust mesh grid warping. *IEEE Transactions on Image Processing* **24**(12), 5260–5273 (2015)
12. Lai, W.S., Huang, J.B., Wang, O., Shechtman, E., Yumer, E., Yang, M.H.: Learning blind video temporal consistency. In: Proceedings of the European conference on computer vision (ECCV). pp. 170–185 (2018)
13. Lee, K.Y., Chuang, Y.Y., Chen, B.Y., Ouhyoung, M.: Video stabilization using robust feature trajectories. In: 2009 IEEE 12th international conference on computer vision. pp. 1397–1404. IEEE (2009)
14. Lee, Y.C., Tseng, K.W., Chen, Y.T., Chen, C.C., Chen, C.S., Hung, Y.P.: 3d video stabilization with depth estimation by cnn-based optimization. In: Proceedings of the IEEE/CVF conference on computer vision and pattern recognition. pp. 10621–10630 (2021)
15. Li, C., Song, L., Chen, S., Xie, R., Zhang, W.: Deep online video stabilization using imu sensors. *IEEE Transactions on Multimedia* **25**, 2047–2060 (2022)
16. Liu, F., Gleicher, M., Jin, H., Agarwala, A.: Content-preserving warps for 3d video stabilization. In: Seminal Graphics Papers: Pushing the Boundaries, Volume 2, pp. 631–639 (2023)
17. Liu, F., Gleicher, M., Wang, J., Jin, H., Agarwala, A.: Subspace video stabilization. *ACM Transactions on Graphics (TOG)* **30**(1), 1–10 (2011)

18. Liu, S., Li, M., Zhu, S., Zeng, B.: Codingflow: Enable video coding for video stabilization. *IEEE Transactions on Image Processing* **26**(7), 3291–3302 (2017)
19. Liu, S., Tan, P., Yuan, L., Sun, J., Zeng, B.: Meshflow: Minimum latency online video stabilization. In: *European Conference on Computer Vision*. pp. 800–815. Springer (2016)
20. Liu, S., Wang, Y., Yuan, L., Bu, J., Tan, P., Sun, J.: Video stabilization with a depth camera. In: *2012 IEEE Conference on Computer Vision and Pattern Recognition*. pp. 89–95. IEEE (2012)
21. Liu, S., Yuan, L., Tan, P., Sun, J.: Bundled camera paths for video stabilization. *ACM transactions on graphics (TOG)* **32**(4), 1–10 (2013)
22. Liu, S., Yuan, L., Tan, P., Sun, J.: Steadyflow: Spatially smooth optical flow for video stabilization. In: *Proceedings of the IEEE conference on computer vision and pattern recognition*. pp. 4209–4216 (2014)
23. Liu, S., Zhang, Z., Liu, Z., Tan, P., Zeng, B.: Minimum latency deep online video stabilization and its extensions. *IEEE Transactions on Pattern Analysis and Machine Intelligence* **47**(2), 1238–1249 (2025). <https://doi.org/10.1109/TPAMI.2024.3493175>
24. Liu, Y.L., Lai, W.S., Yang, M.H., Chuang, Y.Y., Huang, J.B.: Hybrid neural fusion for full-frame video stabilization. In: *Proceedings of the IEEE/CVF International Conference on Computer Vision (ICCV)*. pp. 2299–2308 (October 2021)
25. Liu, Y.L., Lai, W.S., Yang, M.H., Chuang, Y.Y., Huang, J.B.: Hybrid neural fusion for full-frame video stabilization. In: *Proceedings of the IEEE/CVF international conference on computer vision*. pp. 2299–2308 (2021)
26. Matsushita, Y., Ofek, E., Ge, W., Tang, X., Shum, H.Y.: Full-frame video stabilization with motion inpainting. *IEEE Transactions on pattern analysis and Machine Intelligence* **28**(7), 1150–1163 (2006)
27. Mou, C., Wang, X., Xie, L., Wu, Y., Zhang, J., Qi, Z., Shan, Y.: T2i-adapter: Learning adapters to dig out more controllable ability for text-to-image diffusion models. In: *Proceedings of the AAAI conference on artificial intelligence*. vol. 38, pp. 4296–4304 (2024)
28. Peng, Z., Ye, X., Zhao, W., Liu, T., Sun, H., Li, B., Cao, Z.: 3d multi-frame fusion for video stabilization. In: *Proceedings of the IEEE/CVF Conference on Computer Vision and Pattern Recognition*. pp. 7507–7516 (2024)
29. Ravi, N., Reizenstein, J., Novotny, D., Gordon, T., Lo, W.Y., Johnson, J., Gkioxari, G.: Accelerating 3d deep learning with pytorch3d. *arXiv preprint arXiv:2007.08501* (2020)
30. Rombach, R., Blattmann, A., Lorenz, D., Esser, P., Ommer, B.: High-resolution image synthesis with latent diffusion models. In: *Proceedings of the IEEE/CVF conference on computer vision and pattern recognition*. pp. 10684–10695 (2022)
31. Shi, Z., Shi, F., Lai, W.S., Liang, C.K., Liang, Y.: Deep online fused video stabilization. In: *Proceedings of the IEEE/CVF winter conference on applications of computer vision*. pp. 1250–1258 (2022)
32. Teed, Z., Deng, J.: Raft: Recurrent all-pairs field transforms for optical flow. In: *European conference on computer vision*. pp. 402–419. Springer (2020)
33. Wan, T., Wang, A., Ai, B., Wen, B., Mao, C., Xie, C.W., Chen, D., Yu, F., Zhao, H., Yang, J., Zeng, J., Wang, J., Zhang, J., Zhou, J., Wang, J., Chen, J., Zhu, K., Zhao, K., Yan, K., Huang, L., Feng, M., Zhang, N., Li, P., Wu, P., Chu, R., Feng, R., Zhang, S., Sun, S., Fang, T., Wang, T., Gui, T., Weng, T., Shen, T., Lin, W., Wang, W., Wang, W., Zhou, W., Wang, W., Shen, W., Yu, W., Shi, X., Huang, X., Xu, X., Kou, Y., Lv, Y., Li, Y., Liu, Y., Wang, Y., Zhang, Y., Huang, Y., Li,

- Y., Wu, Y., Liu, Y., Pan, Y., Zheng, Y., Hong, Y., Shi, Y., Feng, Y., Jiang, Z., Han, Z., Wu, Z.F., Liu, Z.: Wan: Open and advanced large-scale video generative models (2025), <https://arxiv.org/abs/2503.20314>
34. Wang, M., Yang, G.Y., Lin, J.K., Zhang, S.H., Shamir, A., Lu, S.P., Hu, S.M.: Deep online video stabilization with multi-grid warping transformation learning. *IEEE Transactions on Image Processing* **28**(5), 2283–2292 (2018)
 35. Xu, Y., Zhang, J., Maybank, S.J., Tao, D.: Dut: Learning video stabilization by simply watching unstable videos. *IEEE Transactions on Image Processing* **31**, 4306–4320 (2022)
 36. Yin, S., Wu, C., Liang, J., Shi, J., Li, H., Ming, G., Duan, N.: Dragnuwa: Fine-grained control in video generation by integrating text, image, and trajectory. *arXiv preprint arXiv:2308.08089* (2023)
 37. You, Z., Georgoulis, S., Chen, A., Tang, S., Dai, D.: Gavs: 3d-grounded video stabilization via temporally-consistent local reconstruction and rendering. In: *Proceedings of the Special Interest Group on Computer Graphics and Interactive Techniques Conference Conference Papers*. pp. 1–12 (2025)
 38. Yu, J., Ramamoorthi, R.: Selfie video stabilization. In: *Proceedings of the European conference on computer vision (ECCV)*. pp. 551–566 (2018)
 39. Yu, J., Ramamoorthi, R.: Robust video stabilization by optimization in cnn weight space. In: *Proceedings of the IEEE/CVF Conference on Computer Vision and Pattern Recognition (CVPR)* (June 2019)
 40. Yu, J., Ramamoorthi, R.: Learning video stabilization using optical flow. In: *Proceedings of the IEEE/CVF Conference on Computer Vision and Pattern Recognition (CVPR)* (June 2020)
 41. Yu, M., Hu, W., Xing, J., Shan, Y.: Trajectorycrafter: Redirecting camera trajectory for monocular videos via diffusion models. In: *Proceedings of the IEEE/CVF International Conference on Computer Vision (ICCV)*. pp. 100–111 (October 2025)
 42. Zhang, L., Rao, A., Agrawala, M.: Adding conditional control to text-to-image diffusion models. In: *Proceedings of the IEEE/CVF international conference on computer vision*. pp. 3836–3847 (2023)
 43. Zhang, R., Isola, P., Efros, A.A., Shechtman, E., Wang, O.: The unreasonable effectiveness of deep features as a perceptual metric. In: *Proceedings of the IEEE conference on computer vision and pattern recognition*. pp. 586–595 (2018)
 44. Zhang, Z., Liu, Z., Tan, P., Zeng, B., Liu, S.: Minimum latency deep online video stabilization. In: *Proceedings of the IEEE/CVF International Conference on Computer Vision (ICCV)*. pp. 23030–23039 (October 2023)
 45. Zhao, M., Ling, Q.: Pwstabenet: Learning pixel-wise warping maps for video stabilization. *IEEE Transactions on Image Processing* **29**, 3582–3595 (2020)
 46. Zhao, W., Li, X., Peng, Z., Luo, X., Ye, X., Lu, H., Cao, Z.: Fast full-frame video stabilization with iterative optimization. In: *Proceedings of the IEEE/CVF International Conference on Computer Vision (ICCV)*. pp. 23534–23544 (October 2023)